Published in final edited form as:

Science. 2015 November 20; 350(6263): 985–990. doi:10.1126/science.aac9407.

Patrolling Monocytes Control Tumor Metastasis to the Lung

Richard N. Hanna[1,*], **Caglar Cekic**[2], **Duygu Sag**[3], **Robert Tacke**[1], **Graham D. Thomas**[1], **Heba Nowyhed**[1], **Erica Herrley**[1], **Nicole Rasquinha**[1], **Sara McArdle**[4], **Runpei Wu**[1], **Esther Peluso**[1], **Daniel Metzger**[5], **Hiroshi Ichinose**[6], **Iftach Shaked**[1], **Grzegorz Chodaczek**[4], **Subhra K. Biswas**[7], and **Catherine C. Hedrick**[1,*]

[1]Division of Inflammation Biology, La Jolla Institute for Allergy and Immunology, La Jolla, CA.

[2]Department of Molecular Biology and Genetics, Bilkent University, Ankara, Turkey.

[3]Izmir Biomedicine and Genome Center, Dokuz Eylul University, Izmir, Turkey.

[4]Microscopy Core, La Jolla Institute for Allergy and Immunology, La Jolla, CA.

[5]Department of Functional Genomics and Cancer, Institut de Génétique et de Biologie Moléculaire et Cellulaire (IGBMC), Institut National de Santé et de Recherche Médicale (INSERM U964), Centre National de Recherche Scientifique (CNRS UMR 7104), Université de Strasbourg, Illkirch, France.

[6]Graduate School of Bioscience and Biotechnology, Tokyo Institute of Technology, Yokohama, Japan.

[7]Singapore Immunology Network (SIgN), Agency for Science, Technology & Research A*STAR, Singapore.

Abstract

The immune system plays an important role in regulating tumor growth and metastasis. For example, classical monocytes promote tumorigenesis and cancer metastasis; however, how nonclassical “patrolling” monocytes interact with tumors is unknown. Here we show that patrolling monocytes are enriched in the microvasculature of the lung and reduce tumor metastasis to lung in multiple mouse metastatic tumor models. Nr4a1-deficient mice, which specifically lack patrolling monocytes, showed increased lung metastasis in vivo. Transfer of Nr4a1-proficient patrolling monocytes into Nr4a1-deficient mice prevented tumor invasion in lung. Patrolling monocytes established early interactions with metastasizing tumor cells, scavenged tumor material from the lung vasculature and promoted natural killer cell recruitment and activation. Thus, patrolling monocytes contribute to cancer immunosurveillance and may be targets for cancer immunotherapy.

Monocytes and monocyte-derived macrophages play key roles in tumor progression (1-4). Classical “inflammatory” monocytes ($CCR2^{high}Ly6C^{+}$ in mouse; $CCR2^{high}CD14^{+}CD16^{-}$ in humans) are recruited to tumor sites where they contribute to tumor macrophage content and promote tumor growth and metastasis (5, 6). In contrast, very little is known about the role

[*]**Correspondence to:**rhanna@lji.org and/or hedrick@lji.org.

of nonclassical “patrolling” monocytes (CX3CR1^{high}Ly6C$^{–}$ in mouse; CX3CR1^{high}CD14^{dim}CD16^{+} in humans) in the early growth and metastasis of tumors. Patrolling monocytes (PMo) are involved in the resolution of inflammation; they actively survey the endothelium of the vasculature where they scavenge microparticles and remove cellular debris (7-9). The orphan nuclear receptor Nr4a1 (also known as Nur77/TR3/Ngfi-b) is highly expressed in PMo compared to other immune cells and functions as a master regulator for the development of PMo in mice (10).

To investigate the actions of PMo during early tumor metastasis, we utilized mice expressing green fluorescent protein (GFP) under control of the Nr4a1 promoter (Nr4a1-GFP mice). In these mice, PMo but not Ly6C^{+} classical monocytes, are GFP^{high} (10, 11). We focused our studies on the lung, which is a common site of tumor metastasis and is an important site of PMo activity (12-14). We confirmed that Nr4a1-GFP^{high} cells in the lung were PMo by flow cytometry (fig. S1A-C). Tracking of Nr4a1-GFP^{high} cells by confocal imaging in the lungs identified a large number of Nr4a1-GFP^{high} PMo patrolling the microvasculature (Movie 1, Fig. 1A). Consistent with an important role for PMo in the lung vasculature, we found a 3-4 fold enrichment of Nr4a1-GFP^{high} PMo in the lung compared to other tissues (fig. S1D).

To examine the interactions of PMo with tumor *in vivo*, we imaged Nr4a1-GFP^{high} PMo in the lung after intravenous (IV) injection of Lewis Lung Carcinoma cells expressing red fluorescent protein (LLC-RFP). The number of Nr4a1-GFP^{high} monocytes in the lung increased significantly at 24 hrs following injection of LLC-RFP cells, implying that PMo are actively recruited to the lung tumor environment (Fig. 1A). Within 4 hrs after tumor injection, most Nr4a1-GFP^{high} monocytes decreased patrolling speed in the vasculature, and by 24 hrs they had arrested near lung tumor sites (Fig. 1B). The majority of Nr4a1-GFP^{high} monocytes isolated from lung after LLC tumor transfer maintained their PMo phenotype, which we further confirmed in vitro (Fig. 1C, fig. S1).

Nr4a1-GFP^{high} PMo were recruited to tumor cell clusters within 30 minutes after IV tumor injection, and recruitment continued for at least 7 days (Fig. 1D-E, Movie 2-5). Nr4a1-GFP^{high} cells that were recruited to lung tumor sites were not positive for Ly6C/G (GR-1) in vivo, further confirming that these Nr4a1-GFP^{high} cells are not Ly6G^{+} granulocytes or Ly6C^{+} classical monocytes (Movie 4). The kinetics of PMo recruitment to the lung differed from that of Ly6C^{+} monocytes (fig. S2A). At 7 days, there were significantly higher numbers of Nr4a1-GFP^{high} PMo (~24/100 μm^{3}) associated with tumor areas compared to tumor-free areas, confirming active recruitment of PMo to the tumor (Fig. 1D-E, Movie 5, fig. S1B).

Nr4a1-GFP^{high} monocytes patrolling the vasculature at 4 hrs after tumor injection appeared to move towards and inhibit the attachment of tumor cells to the lung microvasculature (Movie 3). We examined if Nr4a1-GFP^{high} PMo could extravasate outside the vasculature. We found that by 4 hrs post-tumor injection 10-20% of Nr4a1-GFP^{high} PMo had extravasated at tumor sites (fig. S2B-C), and this increased to 40-50% PMo extravasation by 7 days. Together, these findings confirm that PMo establish early immune interactions with tumor cells and can extravasate and accumulate at tumor sites.

In order to determine if PMo have a major role in regulating tumor invasion, metastasis and growth in the lungs *in vivo*, we used Nr4a1-knockout (*Nr4a1*$^{-/-}$) mice, which have a selective loss of PMo (10) (fig. S3). *Nr4a1*$^{-/-}$ mice were IV injected with either syngeneic B16F10 melanoma cells expressing a luciferase reporter or LLC-RFP cells (Fig. 2A-B, fig. S4-5). As early as 24 hrs and up to 21 days after IV injection of B16F10 melanoma, we observed increased tumor invasion in the lungs of *Nr4a1*$^{-/-}$ mice compared to control mice (Fig. 2A-B, fig. S4A-B). We observed no differences in either Ly6C^{+} monocyte or Ly6G^{+} granulocyte populations in the lungs of these mice at 7 days after tumor injection (fig. S4C). B16F10 tumor invasion appeared specific for the lung, as increased tumor metastasis was not observed in the liver (fig S4B). Additionally, increased spontaneous metastases to the lung were observed in *Nr4a1*$^{-/-}$ mice after subcutaneous injection of B16F10 melanoma, suggesting that Nr4a1 expression is important for suppressing primary tumor metastasis to the lung (Fig. 2C). A similar early and sustained increase in lung metastasis in *Nr4a1*$^{-/-}$ mice was also observed after intravenous LLC tumor transfer (fig. S5). We did not detect differences in vascular permeability in the lung between *Nr4a*1$^{-/-}$ and control mice (fig. S6).

We next utilized the MMTV-PyMT model, in which female mice spontaneously develop mammary tumors that metastasize to the lung (15). To focus on Nr4a1 function exclusively in hematopoietic cells, we performed bone marrow transplants using either WT or *Nr4a1*$^{-/-}$ bone marrow transferred into female recipient MMTV-PyMT mice. MMTV-PyMT mice receiving *Nr4a1*$^{-/-}$ bone marrow developed significantly higher numbers of spontaneous metastases to lung, but no differences in primary mammary tumor growth compared to mice receiving WT bone marrow (Fig. 2D-E).

We further tested hematopoietic Nr4a1 function using B16F10 melanoma. Only mice receiving *Nr4a1*$^{-/-}$ bone marrow had increased B16F10 tumor metastases, confirming that Nr4a1 expression in hematopoietic cells regulated tumor cell metastasis to the lung (fig. S7A-B). Analysis of immune cells isolated from lung tumors verified a selective loss of PMo in *Nr4a1*$^{-/-}$ bone marrow transplanted mice (fig. S7C). In the 1:1 chimera mice, equal reconstitution of immune cells from each donor was observed (fig. S7D). However, PMo were derived almost exclusively from WT bone marrow, suggesting that the restoration of the Ly6C^{-} monocyte population prevented tumor metastasis.

To confirm if Nr4a1 expressed in myeloid cells was regulating tumor metastasis to the lung, we examined two different myeloid-specific Nr4a1 conditional knockout models (CSF1R-Cre^{+}*Nr4a1*$^{fl/fl}$ and LysM-Cre^{+}*Nr4a1*$^{fl/fl}$). Deletion of Nr4a1 using CSF1R-Cre^{+}*Nr4a1*$^{fl/fl}$ and LysM-Cre^{+}*Nr4a1*$^{fl/fl}$ mice significantly reduced PMo in circulation (fig. S8), and increased tumor lung metastasis (Fig. 3A-B, fig. S9). Nr4a1 deletion using CSF1R-Cre or LysM-Cre also targets Nr4a1 in macrophages and Ly6C^{+} monocytes, so we cannot completely rule out effects of Nr4a1 in these cells. However, Nr4a1 expression in macrophages and Ly6C^{+} monocytes is relatively low suggesting limited Nr4a1 function (10, 16, 17). No differences in tumor metastasis were observed with T lymphocyte-specific Nr4a1 deletion (fig. S10). Collectively, our studies illustrate increased lung metastasis burden in the absence of Nr4a1 in myeloid cells in multiple cancer models.

To confirm a direct role for PMo in regulating tumor metastasis, wild-type Ly6C$^+$ or Ly6C$^-$ monocytes were adoptively transferred into recipient *Nr4a1*$^{-/-}$ mice prior to tumor injection. A significant number of the transferred monocytes could be found in lung (fig. S11A-B). Reconstitution of PMo into *Nr4a1*$^{-/-}$ mice prevented lung tumor metastasis (Fig. 3C-D). In contrast, transfer of Ly6C$^+$ monocytes into *Nr4a1*$^{-/-}$ mice actually promoted tumor metastasis, consistent with known protumoral properties of this subset of monocytes (5, 18). The majority (80-90%) of transferred Ly6C$^+$ monocytes in circulation did not lose Ly6C expression (fig. S11C). Interestingly, transfer of PMo 24 hrs post-tumor injection into *Nr4a1*$^{-/-}$ mice did not suppress tumor metastasis (fig. S11D), suggesting that PMo need to already be present and active in the vasculature in order to prevent early tumor metastasis. These data directly show that nonclassical PMo inhibit tumor metastasis to the lung.

PMo can act as “intravascular housekeepers” that scavenge microparticles and remove cellular debris from the microvasculature (7). Extracellular vesicles from tumors are important mediators of tumor metastasis, progression and immune suppression, and targeting their removal is an emerging target for cancer therapy (19, 20). We used high-resolution confocal imaging to determine if PMo could engulf and remove tumor material from the lung vasculature. A sizable number of Nr4a1-GFP^{high} PMo containing large amounts of LLC-RFP tumor material were observed at tumor sites in the lung 24 hrs after IV tumor transfer (Fig. 3E). Co-culture assays of mouse PMo with fluorescent-labeled tumor cells confirmed engulfment of large amounts of tumor material (Fig. 3F). Analysis of monocyte populations isolated from the lung at 24 hrs after IV LLC-RFP injection indicated that PMo preferentially took up tumor material, taking up ~5-fold more tumor than did Ly6C$^+$ classical monocytes (Fig. 3G). PMo also preferentially took up significantly more B16F10-YFP tumor material with an average size of 1.39 μm^2, and an average total amount of tumor material per monocyte of 1.92 μm^2 (fig. S12A-B). The homologous human CD14^{dim}CD16$^+$ population of PMo, which similarly has high Nr4a1 expression (8, 21), also engulfed a large quantity of tumor material in vitro, suggesting analogous tumor engulfment function (fig. S12C). Moreover, PMo actively engulfed tumor material within classic endocytic compartments (22)(Fig. 4A). Collectively, these results demonstrate that Nr4a1-dependent PMo rapidly and preferentially endocytose tumor material.

We then asked how PMo recognized tumor cells to prevent metastasis in the lung. The chemokine receptor CX3CR1 is highly expressed on PMo and is important for their arrest at inflammatory sites (fig. S13A) (23-25). CX3CR1-deficient (*Cx3cr1*$^{-/-}$) mice, which also have a significant reduction in PMo, exhibit a similar phenotype to *Nr4a1*$^{-/-}$ mice—of increased tumor burden and metastasis to the lung (26, 27). Though PMo were reduced in numbers in the lung vasculature of *Cx3cr1*$^{-/-}$ mice (about 30-50% reduction, fig. S13B; confirming previous reports) (27), a major proportion of the CX3CR1-deficient PMo remaining were observed patrolling the vasculature as has previously been observed (7). Unlike *Cx3cr1*$^{+/-}$ or WT PMo, *Cx3cr1*$^{-/-}$ PMo did not arrest near LLC tumor cells, and instead remained patrolling within the lung vasculature (Fig. 4B-C, Movie 6). Interestingly, *Cx3cr1*$^{-/-}$ PMo were not recruited to the lung 24 hrs after LLC tumor challenge, while Ly6C$^+$ recruitment was unaffected by loss of CX3CR1 expression (fig. S13B). Importantly, *Cx3cr1*$^{-/-}$ PMo present in the lung showed defective engulfment of tumor material,

indicating that CX3CR1 expression on PMo is critical for mediating the sensing and uptake of tumor material (Fig. 4D).

CX3CL1, a ligand for CX3CR1, has been reported to be high in human and mouse lung (28). Using a CX3CL1-mCherry reporter mouse (29), we found that CX3CL1 was specifically expressed on $CD31^+$ endothelial cells (EC) at low levels in the lung microvasculature (Fig. 4E-F, fig. S13C). CX3CL1 expression was most prevalent in lung EC compared to EC in other tissues (fig. S13D), which may partially explain the enrichment and preferential function of PMo in the lung. CX3CL1 expression on lung EC increased in response to tumor challenge (Fig. 4E), and at sites of lung tumor metastasis (Fig 4F), consistent with reports of increased CX3CL1 during lung inflammation (30).

TLR7 has been linked to recruitment of PMo in response to kidney damage in mice (7). However, we found that TLR7 did not play a significant role in either recruitment of PMo to the lung after tumor injection (fig. S13B), or in the uptake of tumor material by PMo (Fig. 4D). We conclude that both CX3CR1 expression on monocytes and CX3CL1 expression by EC are critical for recruitment of PMo to sites of tumor extravasation to mediate the removal of tumor material from the lung. CX3CL1 expression by tumor cells (31) may also drive monocyte recruitment. In agreement with our findings, many studies have reported that CX3CL1 expression by either tumor cells or by tumor-associated cells is anti-tumoral and correlated with good prognosis (32-34). However, the function of the CX3CL1/CX3CR1 axis, particularly during later stages of tumor growth, is complex (35, 36).

Finally, we examined whether PMo can directly kill tumor cells. After multiple attempts using various experimental conditions, direct killing of tumor cells by PMo was not observed (fig. S14). However, PMo may be important for antibody-dependent cell-mediated cytotoxicity of either tumor cells or suppressive immune cells within the tumor environment (37, 38). In response to IV injected B16F10 tumor, PMo isolated from lung produced significantly higher levels of natural killer (NK) cell activation and recruitment-related chemokines CCL3, CCL4 and CCL5 compared to classical $Ly6C^+$ monocytes (Fig. 4G)(39, 40). Correlating with this finding, myeloid-specific Nr4a1 knockout mice ($CSF1R\text{-}Cre^+$*Nr4a1*$^{fl/fl}$) showed reduced NK cell recruitment to the lung in response to tumor (Fig. 4H), suggesting that PMo controlled the recruitment of NK cells to tumor sites. A similar reduction in NK cell recruitment, and CD44 activation (fig. S15A-B) was also found in lungs of PyMT mice that received Nr4a1-deficient bone marrow. However, Nr4a1 does not regulate NK cell development (fig. S15C). Uptake of tumor material by PMo does not require the presence of NK cells (fig. S16A-B). Importantly, NK cell depletion reduced the differences in metastasis between WT and $CSF1R\text{-}Cre^+Nr4a1^{fl/fl}$ mice (fig. S16C). Thus, PMo inhibit metastasis, at least in part, through the regulation of NK cell recruitment and activity.

In summary, we demonstrate a cancer surveillance role of PMo wherein they prevent tumor metastasis to lung. PMo are actively recruited to lung metastasis sites in a CX3CR1-dependent manner, where they function to scavenge tumor material as well as recruit and activate NK cells that leads to the prevention of tumor cell metastasis (fig. S17). Selective

targeting by increasing PMo activity and/or their regulation by Nr4a1 may represent a novel therapy for preventing cancer metastasis to the lung.

Supplementary Material

Refer to Web version on PubMed Central for supplementary material.

Acknowledgements

The authors would like to thank K. Ley and H. Shaked for critically reviewing and editing this manuscript, K. Hogquist for Nr4a1-GFP reporter mice, M. Kronenberg for B16F10 melanoma cells, A. Blatchley and D. Yoakum for assistance with mouse colony management, A. Strasner for help establishing tumor models, and Z. Mikulski for his assistance with imaging. The data presented in this manuscript are tabulated in the main paper and in the supplementary materials. Nr4a1-floxed conditional mice are available from IGBMC under a material transfer agreement with D. Metzger and H. Ichinose. C. Hedrick, R. Hanna and LJI have filed a U.S. patent application (US 13/646,183) that relates to specific topic “Methods and Uses of Nur77 and Nur77 Agonists to Modulate Macrophages and Monocytes, and Treat Inflammation, Inflammatory Disease and Cardiovascular Disease” and an invention disclosure that relates to the specific topic “Patrolling Monocytes Control Tumor Metastasis to the Lung”. This work was supported by NIH R01 HL118765 and NIH R01 CA202987 (both to C.C.H.), an American Heart Association Postdoctoral Award 3POST16990029 (to R.T.), an NIH F32 postdoctoral fellowship NIH F32 HL117533-02 (to H.N.), an American Heart Association Scientist Development Grant 125SDG12070005 (to R.N.H.) and the LJI Board of Directors Fellowship (to R.N.H.), the Centre National pour la Recherche Scientifique (CNRS) and the Institut National de la Santé et de la Recherche Médicale (INSERM) (to D.M.), and core-funding from Singapore Immunology Network (A*STAR) (to S.K.B.).

References

1. Biswas SK, Mantovani A. Macrophage plasticity and interaction with lymphocyte subsets: cancer as a paradigm. Nat Imunol. Oct.2010 11:889.
2. Murray PJ, Wynn TA. Protective and pathogenic functions of macrophage subsets. Nat Rev Immunol. Nov.2011 11:723. [PubMed: 21997792]
3. Wynn TA, Chawla A, Pollard JW. Macrophage biology in development, homeostasis and disease. Nature. Apr.2013 496:445. [PubMed: 23619691]
4. Franklin RA, et al. The cellular and molecular origin of tumor-associated macrophages. Science. May.2014 344:921. [PubMed: 24812208]
5. Qian BZ, et al. CCL2 recruits inflammatory monocytes to facilitate breast-tumour metastasis. Nature. Jul 14.2011 475:222. [PubMed: 21654748]
6. Movahedi K, et al. Different tumor microenvironments contain functionally distinct subsets of macrophages derived from Ly6C(high) monocytes. Cancer Res. Jul.2010 70:5728. [PubMed: 20570887]
7. Carlin LM, et al. Nr4a1-dependent Ly6C(low) monocytes monitor endothelial cells and orchestrate their disposal. Cell. Apr 11.2013 153:362. [PubMed: 23582326]
8. Cros J, et al. Human CD14dim monocytes patrol and sense nucleic acids and viruses via TLR7 and TLR8 receptors. Immunity. Sep 24.2010 33:375. [PubMed: 20832340]
9. Auffray C, et al. Monitoring of blood vessels and tissues by a population of monocytes with patrolling behavior. Science. Aug.2007 317:666. [PubMed: 17673663]
10. Hanna RN, et al. The transcription factor NR4A1 (Nur77) controls bone marrow differentiation and the survival of Ly6C-monocytes. Nat Immunol. Aug.2011 12:778. [PubMed: 21725321]
11. Moran AE, et al. T cell receptor signal strength in Treg and iNKT cell development demonstrated by a novel fluorescent reporter mouse. J Exp Med. May.2011
12. Landsman L, Jung S. Lung macrophages serve as obligatory intermediate between blood monocytes and alveolar macrophages. J Immunol. Sep.2007 179:3488. [PubMed: 17785782]
13. Landsman L, Varol C, Jung S. Distinct differentiation potential of blood monocyte subsets in the lung. J Immunol. Feb.2007 178:2000. [PubMed: 17277103]

14. Jakubzick C, et al. Blood monocyte subsets differentially give rise to CD103+ and CD103- pulmonary dendritic cell populations. J Immunol. Mar.2008 180:3019. [PubMed: 18292524]
15. Guy CT, Cardiff RD, Muller WJ. Induction of mammary tumors by expression of polyomavirus middle T oncogene: a transgenic mouse model for metastatic disease. Mol Cell Biol. Mar.1992 12:954. [PubMed: 1312220]
16. Saeed S, et al. Epigenetic programming of monocyte-to-macrophage differentiation and trained innate immunity. Science. Sep.2014 345:1251086. [PubMed: 25258085]
17. Jojic V, et al. Identification of transcriptional regulators in the mouse immune system. Nat Immunol. Jun.2013 14:633. [PubMed: 23624555]
18. Sanford DE, et al. Inflammatory Monocyte Mobilization Decreases Patient Survival in Pancreatic Cancer: A Role for Targeting the CCL2/CCR2 Axis. Clin Cancer Res. Jul.2013 19:3404. [PubMed: 23653148]
19. Vader P, Breakefield XO, Wood MJ. Extracellular vesicles: emerging targets for cancer therapy. Trends Mol Med. Apr.2014
20. Pucci F, Pittet MJ. Molecular pathways: tumor-derived microvesicles and their interactions with immune cells in vivo. Clin Cancer Res. May.2013 19:2598. [PubMed: 23426276]
21. Hanna RN, et al. NR4A1 (Nur77) deletion polarizes macrophages toward an inflammatory phenotype and increases atherosclerosis. Circulation research. Feb 3.2012 110:416. [PubMed: 22194622]
22. Please see detailed methods for this experiment in the Materials and Methods section of Supplementary Materials.
23. Thomas G, Tacke R, Hedrick CC, Hanna RN. Nonclassical patrolling monocyte function in the vasculature. Arterioscler Thromb Vasc Biol. Jun.2015 35:1306. [PubMed: 25838429]
24. Jung S, et al. Analysis of fractalkine receptor CX(3)CR1 function by targeted deletion and green fluorescent protein reporter gene insertion. Mol Cell Biol. Jun.2000 20:4106. [PubMed: 10805752]
25. Geissmann F, Jung S, Littman DR. Blood monocytes consist of two principal subsets with distinct migratory properties. Immunity. Jul.2003 19:71. [PubMed: 12871640]
26. Yu YR, et al. Defective antitumor responses in CX3CR1-deficient mice. International journal of cancer. Journal international du cancer. Jul 15.2007 121:316. [PubMed: 17372897]
27. Landsman L, et al. CX3CR1 is required for monocyte homeostasis and atherogenesis by promoting cell survival. Blood. Jan.2009 113:963. [PubMed: 18971423]
28. Su AI, et al. A gene atlas of the mouse and human protein-encoding transcriptomes. Proceedings of the National Academy of Sciences of the United States of America. Apr 20.2004 101:6062. [PubMed: 15075390]
29. Kim KW, et al. In vivo structure/function and expression analysis of the CX3C chemokine fractalkine. Blood. Nov.2011 118:e156. [PubMed: 21951685]
30. Zhang J, Patel JM. Role of the CX3CL1-CX3CR1 axis in chronic inflammatory lung diseases. International journal of clinical and experimental medicine. 2010; 3:233. [PubMed: 20827321]
31. Ferretti E, Pistoia V, Corcione A. Role of fractalkine/CX3CL1 and its receptor in the pathogenesis of inflammatory and malignant diseases with emphasis on B cell malignancies. Mediators of inflammation. 2014; 2014:480941. [PubMed: 24799766]
32. Hyakudomi M, et al. Increased expression of fractalkine is correlated with a better prognosis and an increased number of both CD8+ T cells and natural killer cells in gastric adenocarcinoma. Annals of surgical oncology. Jun.2008 15:1775. [PubMed: 18363071]
33. Kee JY, et al. Antitumor immune activity by chemokine CX3CL1 in an orthotopic implantation of lung cancer model. Molecular and clinical oncology. Jan.2013 1:35. [PubMed: 24649119]
34. Park MH, Lee JS, Yoon JH. High expression of CX3CL1 by tumor cells correlates with a good prognosis and increased tumor-infiltrating CD8+ T cells, natural killer cells, and dendritic cells in breast carcinoma. Journal of surgical oncology. Sep 15.2012 106:386. [PubMed: 22422195]
35. Schmall A, et al. Macrophage and cancer cell cross-talk via CCR2 and CX3CR1 is a fundamental mechanism driving lung cancer. American journal of respiratory and critical care medicine. Feb 15.2015 191:437. [PubMed: 25536148]

36. Tardaguila, M.; Manes, S. Oncology: Theory and Practice: The Complex Role of Chemokines in Cancer: The Case of the CX3CL1-CX3CR1 Axis. iConcept Press, Ltd.; 2014.

37. Romano E, et al. Ipilimumab-dependent cell-mediated cytotoxicity of regulatory T cells ex vivo by nonclassical monocytes in melanoma patients. Proceedings of the National Academy of Sciences of the United States of America. May.2015 112:6140. [PubMed: 25918390]

38. Szaflarska A, et al. Antitumor response of CD14+/CD16+ monocyte subpopulation. Experimental hematology. Aug.2004 32:748. [PubMed: 15308326]

39. Maghazachi AA. Role of chemokines in the biology of natural killer cells. Curr Top Microbiol Immunol. 2010; 341:37. [PubMed: 20369317]

40. Robertson MJ. Role of chemokines in the biology of natural killer cells. J Leukoc Biol. Feb.2002 71:173. [PubMed: 11818437]

41. Lee S, et al. Unimpaired thymic and peripheral T cell death in mice lacking the nuclear receptor NGFI-B (Nur77). Science. Jul.1995 269:532. [PubMed: 7624775]

42. Davie SA, et al. Effects of FVB/NJ and C57Bl/6J strain backgrounds on mammary tumor phenotype in inducible nitric oxide synthase deficient mice. Transgenic research. Apr.2007 16:193. [PubMed: 17206489]

43. Deng L, et al. A novel mouse model of inflammatory bowel disease links mammalian target of rapamycin-dependent hyperproliferation of colonic epithelium to inflammation-associated tumorigenesis. Am J Pathol. Feb.2010 176:952. [PubMed: 20042677]

44. Sekiya T, et al. The nuclear orphan receptor Nr4a2 induces Foxp3 and regulates differentiation of CD4+ T cells. Nat Commun. 2011; 2:269. [PubMed: 21468021]

45. Thornton EE, Krummel MF, Looney MR. Live imaging of the lung. Curr Protoc Cytom. Apr.2012 Chapter 12, Unit12.28.

46. McArdle S, Chodaczek G, Ray N, Ley K. Intravital live cell triggered imaging system reveals monocyte patrolling and macrophage migration in atherosclerotic arteries. J Biomed Opt. Feb.2015 20:26005. [PubMed: 25710308]

47. McArdle, S., SA.; Ley, K.; Ray, N. paper presented at the IEEE International Conference on Image Processing; Paris, France. 2014;

48. Wallace KL, Linden J. Adenosine A2A receptors induced on iNKT and NK cells reduce pulmonary inflammation and injury in mice with sickle cell disease. Blood. Dec.2010 116:5010. [PubMed: 20798237]

One Sentence Summary

Nonclassical patrolling monocytes aid in cancer surveillance by preventing tumor metastasis to the lung.

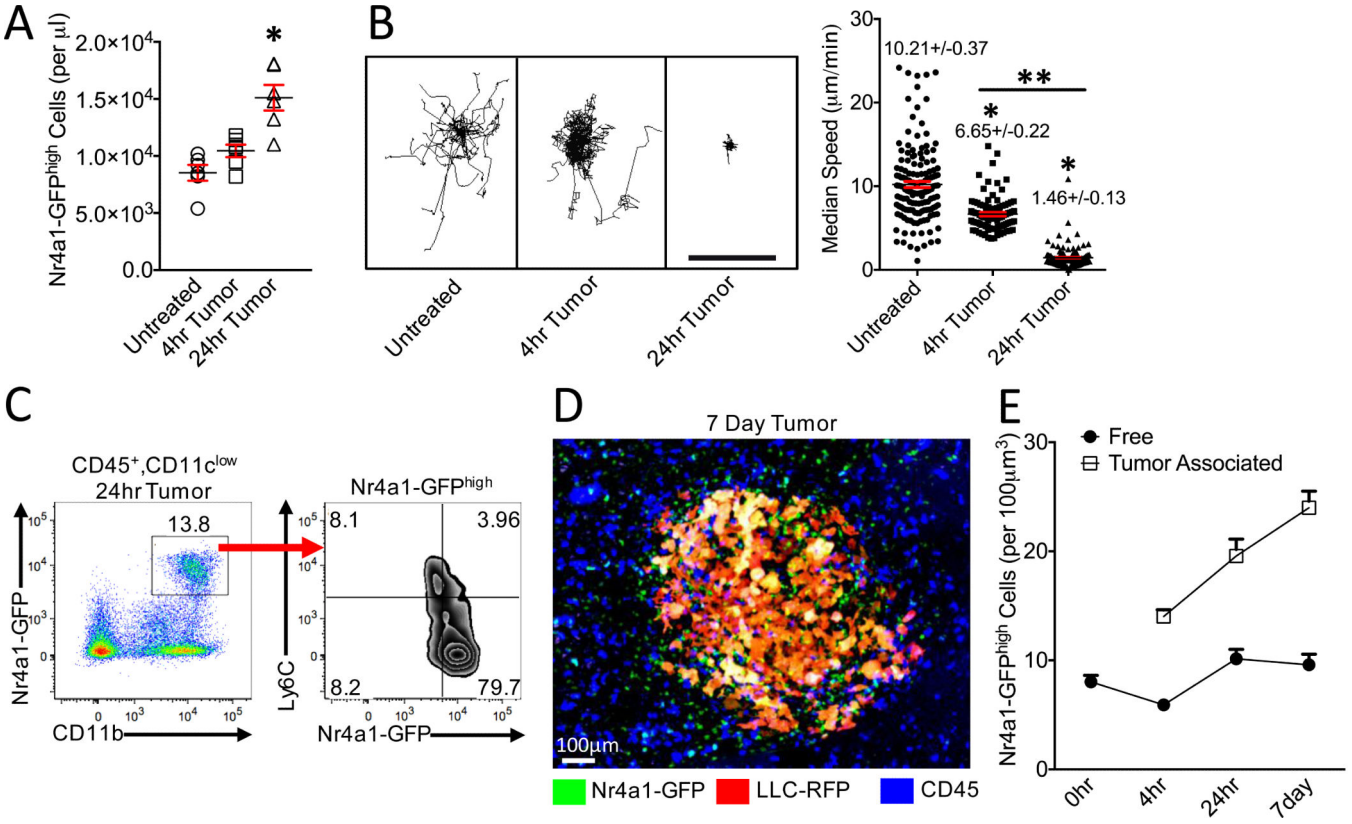

Fig. 1. Nr4a1-GFP^{high} monocytes patrol the vasculature, and interact with tumor in the lung

(A) Quantification of Nr4a1-GFP^{high} PMo per µl of blood volume in lung (Untreated), 4 hrs or 24 hrs after IV LLC-RFP transfer (n=5 mice per group). (B) Quantification of Nr4a1-GFP^{high} monocyte movement in lung before (Untreated), 4 hrs or 24 hrs after LLC-RFP tumor injection. Monocyte tracks transposed to a common origin from a representative 20 min movie (left, scale bar=100 µm), and quantification of median speed of monocytes (right, combined speed data from analysis of 3 separate mice; *=p<0.001 lower than untreated; **=p<0.001 than 4hr tumor). (C) Representative gating of Nr4a1-GFP^{high}CD11b^{+} cells from all Live CD45^{+}CD11c^{low} cells 24 hrs after IV LLC-RFP transfer. (D) Representative confocal image of Nr4a1-GFP^{high} monocytes (Green) interacting with LLC-RFP cells (Red) in the lung 7 days after IV LLC-RFP transfer. Immune cells in the vasculature were labeled with IV injected anti-CD45 antibody (Blue). (E) Quantification of free (>100 µm from tumor site) and tumor-associated (<50 µm from tumor site) Nr4a1-GFP^{high} monocytes in the lung at various time points after tumor injection (combined analysis of 5 mice per group; p<0.01 for each tumor-associated area compared to free tumor area for each time point).

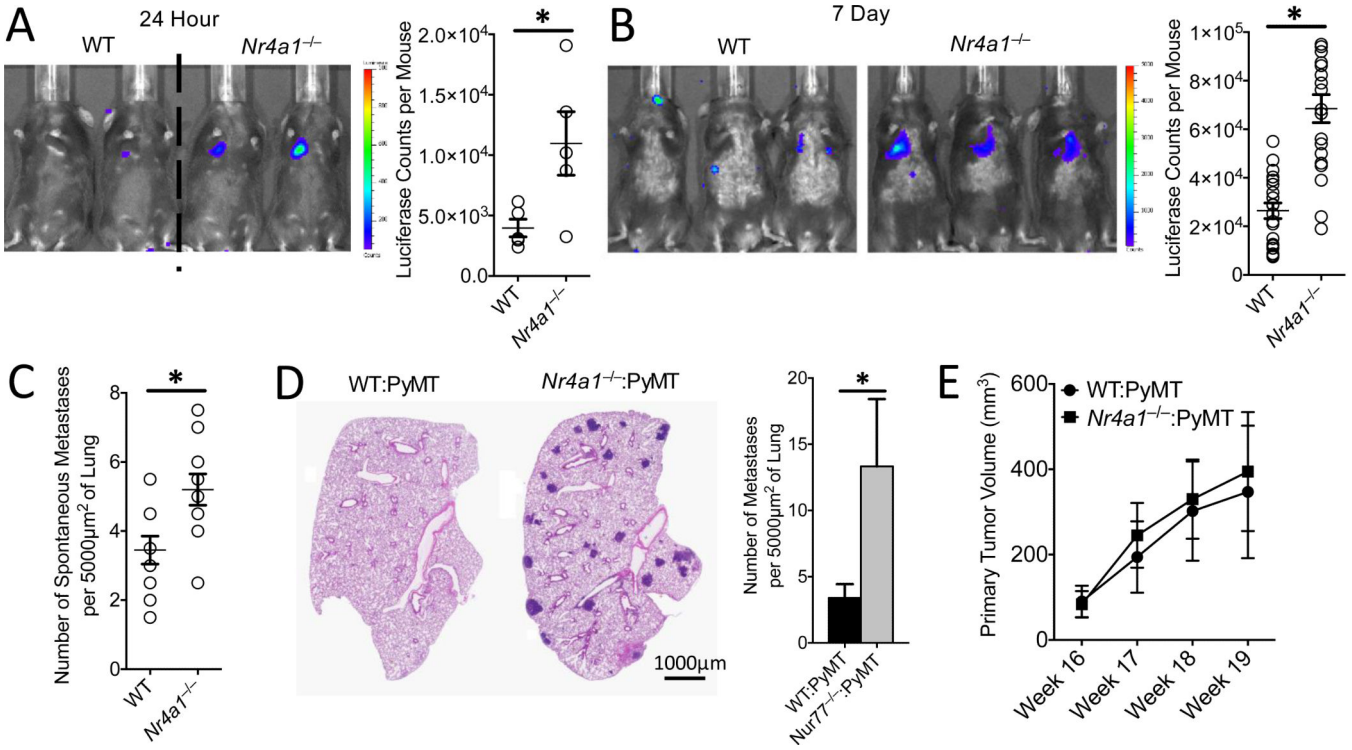

Fig. 2. Increased lung metastasis of tumors in *Nr4a1*$^{-/-}$ mice

(A) *In vivo* luciferase detection in wild-type control (WT) and *Nr4a1*$^{-/-}$ mice 24 hrs after IV injection of 5×10^5 B16F10 melanoma cells expressing luciferase (Left) and quantification (Right) (*=p<0.03, representative experiment with 5 mice per group). (B) *In vivo* luciferase detection (Left), and quantification (Right), in WT and *Nr4a1*$^{-/-}$ mice 7 days after IV injection with 3×10^5 B16F10-luciferase cells (*=p<0.001, n=18 mice per group combined from 3 separate experiments). (C) Number of spontaneous tumor metastases per 5000 μm^2 of lung surface 28 days after SubQ injection of 1×10^5 B16F10-YFP cells (*=p<0.01, n=7 mice per group). (D-E) Lung tumor metastasis in MMTV-PyMT mice reconstituted with WT (WT:PyMT) or *Nr4a1*$^{-/-}$ (Nr4a1$^{-/-}$:PyMT) bone marrow. (D) Representative MMTV-PyMT mouse lung histology stained with hematoxylin and eosin (Left), and quantification of number of spontaneous lung metastases per 5000 μm^2 of lung surface (Right). *=p<0.05 n=12 for WT and n=15 for *Nr4a1*$^{-/-}$. (E) Quantification of primary breast tumor growth in MMTV-PyMT mice. N=12 for WT and n=15 for *Nr4a1*$^{-/-}$.

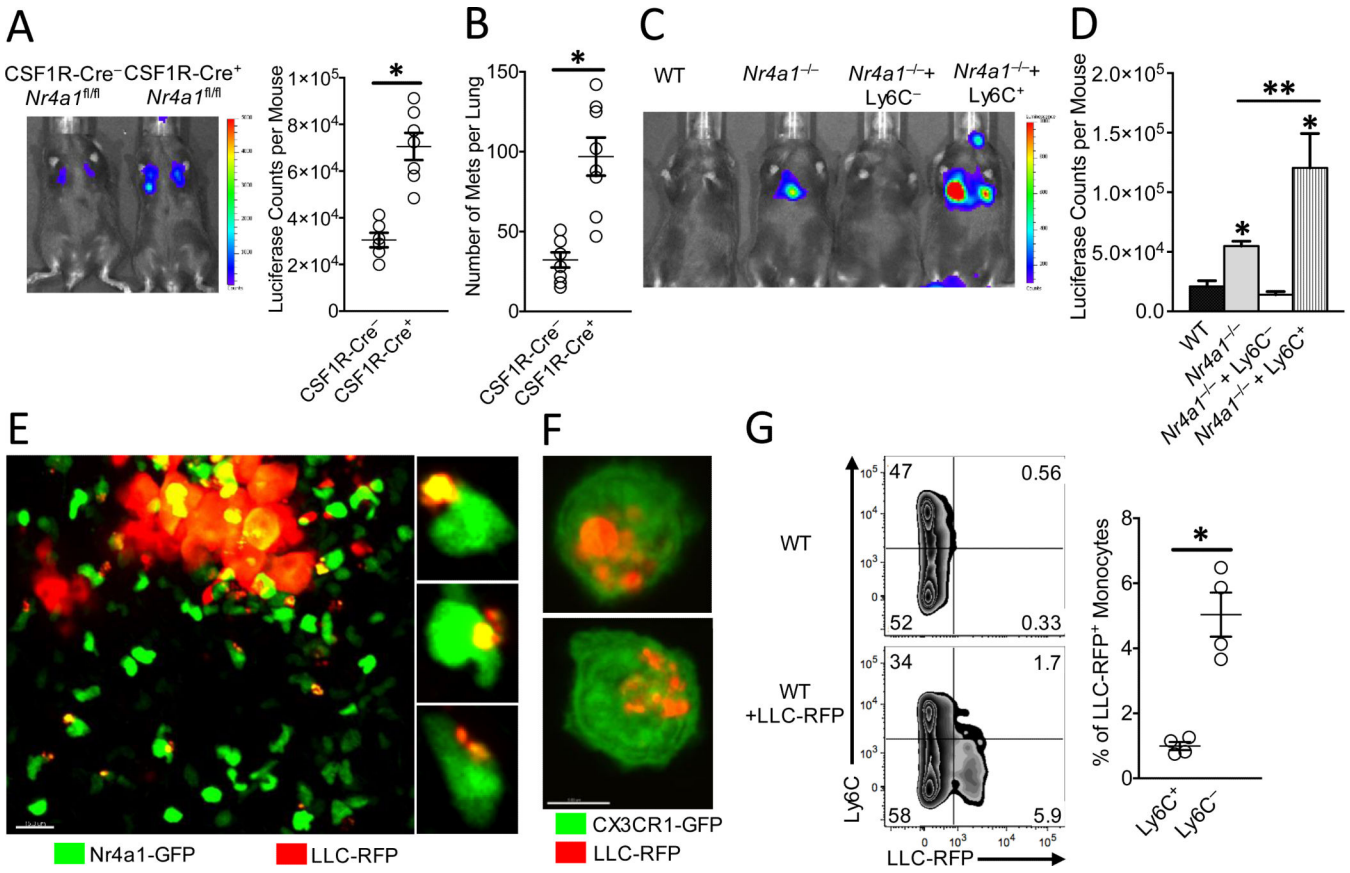

Fig. 3. Nr4a1-expressing patrolling monocytes reduce tumor metastasis and engulf tumor material in the lung

(A) *In vivo* imaging (Left), and quantification (Right) of tumor in lungs of CSF1R-Cre^{-}*Nr4a1*$^{fl/fl}$ (CSF1R-Cre^{-}) or CSF1R-Cre^{+}*Nr4a1*$^{fl/fl}$ (CSF1R-Cre^{+}) mice 7 days after IV injection of 3×10^{5} B16F10-luciferase tumor cells (n=6 mice per group, *=p<0.01; experiment replicated 2 times). (B) Quantification of the number of tumor metastases per lungs of CSF1R-Cre^{-}*Nr4a1*$^{fl/fl}$ (CSF1R-Cre^{-}) and CSF1R-Cre^{+}*Nr4a1*$^{fl/fl}$ (CSF1R-Cre^{+}) mice 7 days after IV injection of 3×10^{5} B16F10-YFP tumor cells (n=8 mice per group, *=p<0.01). (C-D) *Nr4a1*$^{-/-}$ mice were injected IV with 5×10^{5} wild-type Ly6C^{-} PMo, Ly6C^{+} inflammatory monocytes, or PBS at day 0. On day 1, 3×10^{5} B16F10-luciferase tumor cells were injected IV and tumor metastasis and growth were measured by *in vivo* imaging at day 8. Representative *in vivo* imaging (C), and quantification (D) of B16F10-luciferase metastasis 8 days after monocyte transfer and 7 days after tumor transfer in wild-type (WT) or *Nr4a1*$^{-/-}$ mice. (Combined data from 5 separate experiments with n=2 mice per group; *=p<0.01 statistically different than WT; **=p<0.05 statistically different than *Nr4a1*$^{-/-}$). (E) Imaging of tumor material uptake in lung by Nr4a1-GFP^{high} monocytes 24 hrs after IV injection of LLC-RFP tumor cells. Representative higher magnification images to right. (F) Uptake of LLC-RFP tumor material by CX3CR1-GFP^{high}Ly6C^{-} PMo after 24 hrs of co-culture. Note that Nr4a1-GFP expression is primarily nuclear so monocyte cell membranes are not visible in images (G) Representative flow plot (Left) and quantification (Right) of tumor material uptake by all monocytes in the lung 24 hrs after IV tumor injection of 3×10^{5} LLC-RFP cells (n=4 mice per goup; *=p<0.01; experiment replicated 3 times).

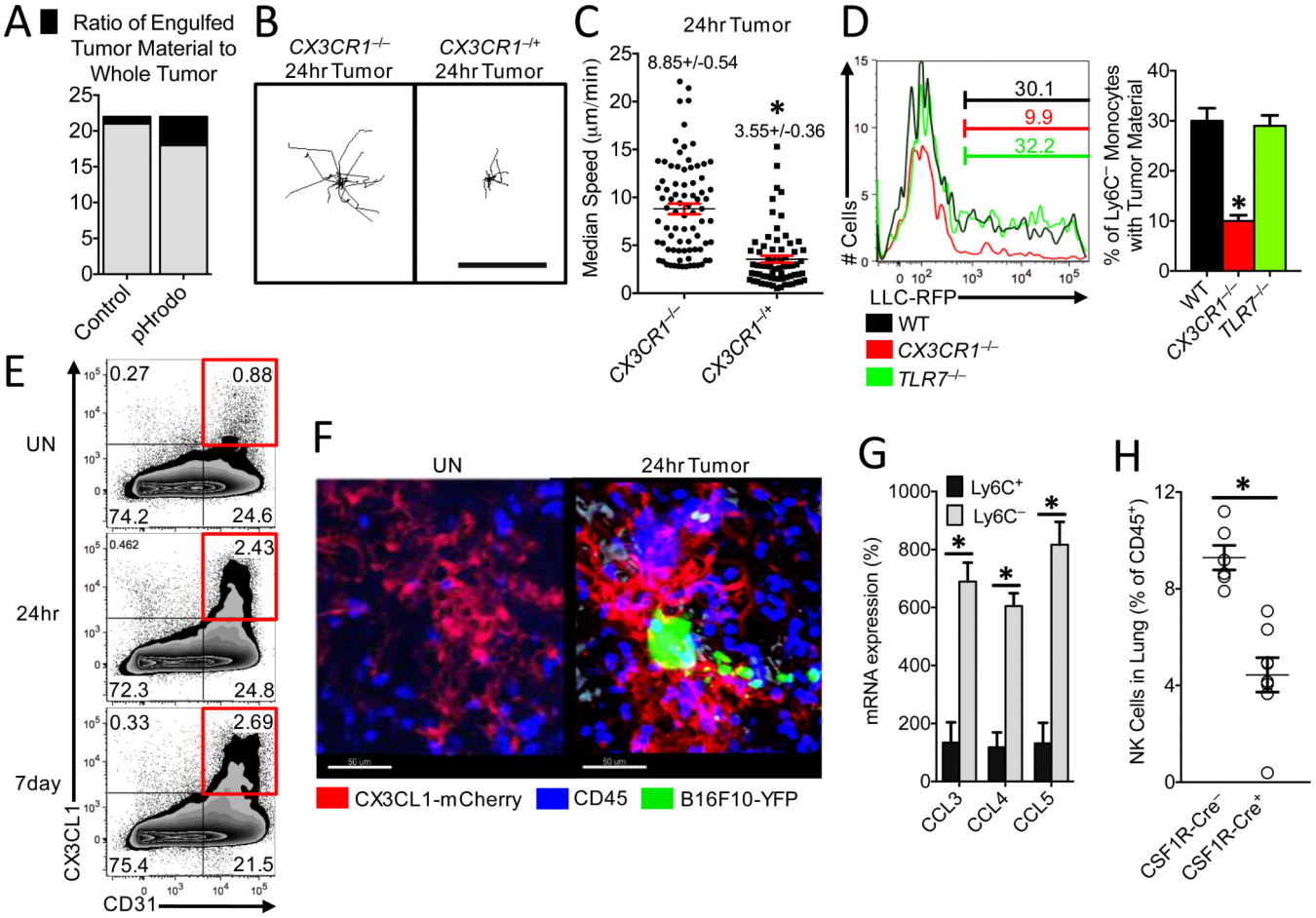

Fig. 4. Patrolling monocytes detect tumor material in a CX3CR1-dependent manner and recruit NK cells to the lung tumor environment

(A) Ratio of fluorescent intensity of tumor material engulfed by PMo (black) to fluorescent intensity of whole tumor (black and grey) 3 hrs after IV LLC tumor injection. LLC tumors were labeled with either CellTrace Violet control dye (Control) or a pH-sensitive pHrodo Red dye (pHrodo) and then IV injected in a 1:1 ratio into a wild-type mouse (n=3 mice per group of representative experiment replicated 3 times). Representative tracking (B) and median speed (C) of *Cx3cr1*$^{-/-}$ *or Cx3cr1*$^{-/+}$ monocyte movement 24 hrs after IV tumor injection in the lung. Monocyte tracks transposed to a common origin from representative 20 min movies (scale bar=100 μm, representative tracks shown from one mouse, median speed calculated from tumor areas analyzed in 3 separate mice per group, *=p<0.001). (D) Percentage of Ly6C^{-} PMo containing LLC-RFP tumor material in the lung 3 hrs after IV injection of tumor into representative wild-type (WT), *Cx3cr1*$^{-/-}$, or *Tlr7*$^{-/-}$ mice (left), and quantification of tumor material uptake (right) (n=3 per group; *p<0.001 versus WT). (E) Percentage of CD31^{+} CX3CL1^{+} lung endothelial cells isolated from Untreated (UN) or 24 hrs or 7 days after IV injection of B16F10-YFP tumor cells into CX3CL1-mCherry mice. (F) Representative imaging of CX3CL1-mCherry (Red) expression in lung 24 hrs after IV injection of B16F10-YFP tumor cells (Green) in CX3CL1-mCherry mice. CD45^{+} immune cells are labeled in blue. (G) Relative chemokine mRNA expression in Ly6C^{+} or Ly6C^{-} monocytes isolated from lung by FACS 24 hrs after IV B16F10 tumor injection (monocyte

populations isolated from three separate mice; *=p<0.01; experiment repeated 3 times). (H) Percentage of natural killer (NK) cells in the lungs of CSF1R-Cre^{-}Nr4a1$^{fl/fl}$ (CSF1R-Cre^{-}) or CSF1R-Cre^{+}Nr4a1$^{fl/fl}$ (CSF1R-Cre^{+}) mice 7 days after IV injection of 3×10^{5} B16F10-luciferase tumor cells (n=6 mice per group, *=p<0.01).